



Graphene and SESAM mode-locked Yb:CNCS lasers with self-frequency doubling properties

MACIEJ KOWALCZYK,^{1,2,*} XUZHAO ZHANG,^{3,4} XAVIER MATEOS,³ SHIYI GUO,⁴ ZHENGPING WANG,⁴ XINGUANG XU,⁴ PAVEL LOIKO,⁵ JI EUN BAE,⁶ FABIAN ROTERMUND,⁶ JAROSŁAW SOTOR,¹ UWE GRIEBNER,² AND VALENTIN PETROV²

¹Laser & Fiber Electronics Group, Faculty of Electronics, Wrocław University of Science and Technology, Wybrzeże Wyspiańskiego 27 50-370, Wrocław, Poland

²Max Born Institute for Nonlinear Optics and Short Pulse Spectroscopy, Max-Born-Str. 2a D-12489, Berlin, Germany

³Universitat Rovira i Virgili, Depart. Química Física i Inorgànica, FiCMA-FiCNA-EMaS, Campus Sescelades E-43007, Tarragona, Spain

⁴State Key Laboratory of Crystal Materials and Institute of Crystal Materials, Shandong University 250100, Jinan, China

⁵ITMO University, 49 Kronverkskiy Pr., 197101, St. Petersburg, Russia

⁶Department of Physics, KAIST, Daehak-ro 291, Yuseong-gu 34141, Daejeon, South Korea
[*m.kowalczyk@pwr.edu.pl](mailto:m.kowalczyk@pwr.edu.pl)

Abstract: We report on mode-locking of an Yb:Ca₃NbGa₃Si₂O₁₄ laser, which is pumped by a fiber-coupled single-mode laser diode. The shortest pulse duration obtained with a semiconductor saturable absorber mirror is 52 fs, with 75 mW of average output power. Sub-60 fs operation tunable between 1055 and 1074 nm is achieved by employing semiconductor absorbers with different characteristics. We also demonstrate passive mode-locking results with transmissive graphene saturable absorber, reaching an 85 fs pulse duration with 23 mW output power. Moreover, we present the non-phase-matched self-frequency doubling properties of this non-centrosymmetric crystal in the femtosecond regime.

© 2019 Optical Society of America under the terms of the [OSA Open Access Publishing Agreement](#)

1. Introduction

Calcium niobium gallium silicate (Ca₃NbGa₃Si₂O₁₄, shortly CNCS) is a langasite-type silicate crystal, which has been primarily studied mostly because of its potential in piezoelectric applications [1,2]. Recently, this ordered, trigonal crystal has also drawn the attention of the laser community. Initially, CNCS was investigated as a host matrix for neodymium (Nd³⁺) doping in continuous wave (CW) [3–5], passively Q-switched [6] and mode-locked (ML) lasers [7]. Subsequently, the first ytterbium (Yb³⁺) doped CNCS crystal has been presented [8]. A detailed spectroscopic characterization of Yb³⁺:CNCS for various doping levels has been performed in [9,10] and such crystals were employed in CW lasers optimized for operation at the 1 μm fundamental wavelength. Using a compact microchip-type cavity configuration, the laser delivered up to 7.3 W of average output power with an excellent slope efficiency of 78% [9]. Yb:CNCS exhibits very broad (~50 nm) and smooth gain cross-section spectrum, which makes it very attractive for a broadband ML operation.

Due to its non-centrosymmetric structure (trigonal symmetry, point group 32), CNCS exhibits second order nonlinearity. This positive uniaxial crystal possesses sufficient birefringence for realization of self-frequency doubled (SFD) lasers based on the Nd³⁺ [6] and Yb³⁺ [8] emission near 1 μm. However, SFD has not been demonstrated in the femtosecond regime, yet. Nonzero $\chi^{(2)}$ nonlinearity is a very interesting property concerning ML lasers, as it enables to obtain ultrashort green pulses [11]. Additionally, it allows one to exploit the cascaded $\chi^{(2)}$ mechanism, introducing negative self-phase modulation. Consequently, it can be

employed as a mode-locking and soliton type compression technique [12–14]. The number of SFD Yb-doped crystals is remarkably limited, with highest second-harmonic powers achieved with borates such as Yb:YAl₃(BO₃)₄ (Yb:YAB) and Yb:Ca₄Y(BO₃)₃ (Yb:YCOB) [15–18]. Most of the performed experiments concerned solely the CW regime and there are very few demonstrations of femtosecond SFD laser oscillators operating at 1 μm [11,19].

In this paper, we present first results with an Yb:CNGS passively ML oscillator employing two types of saturable absorbers: semiconductor saturable absorber mirror (SESAM) and graphene saturable absorber (GSA). The crystal was pumped by a single-mode laser diode, generating pulses as short as 52 and 85 fs, for the SESAM and GSA ML operation, respectively. Ultrafast operation with tunability between 1055 and 1074 nm was achieved by applying SESAMs with different parameters. We also characterized the self-frequency doubling in the mode-locking regime without phase-matching.

2. Experimental setup

The scheme of the X-shaped cavity is depicted in Fig. 1. The *c*-cut 5 at. % Yb:CNGS sample was 2.7 mm thick. It was uncoated and inclined under Brewster's angle with the *c*- and one of its *a*-axes in the horizontal plane. Details of the growth procedure as well as the spectroscopic properties for this doping level can be found in [9,10]. The crystal was placed between two folding curved mirrors ($M_{1,2}$) forming a waist with a size of $22 \times 42 \mu\text{m}$ (Gaussian radius at sagittal and tangential plane; calculated with ABCD matrix formalism). It was pumped by a single-mode fiber-coupled laser diode, which delivered up to 1050 mW of polarized radiation with an excellent beam quality. The pump beam was reimaged with an 18.4 mm aspheric lens and a 100 mm spherical lens, which resulted in a measured beam radius of $22 \mu\text{m}$. Due to the relatively low pump power cooling of the gain medium was not necessary and it was not provided. The pump wavelength of 980 nm is located close to the peak absorption of the crystal (double peak at 977 nm and 979.1 nm [10]). The Yb:CNGS absorption at maximum pump power was measured to be about 75% and 45% for lasing and non-lasing conditions, respectively. Two output couplers (OCs) with transmissions of 0.4% and 2.6% were used.

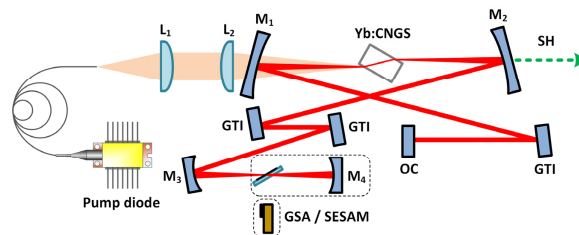


Fig. 1. Experimental setup of the ML Yb:CNGS laser. L_1 —18.4 mm aspheric lens; L_2 —100 mm spherical lens; $M_{1,2}$ —dichroic concave mirrors (RoC = -100 mm); M_3 —HR concave mirror (RoC = -100 mm); M_4 —HR concave mirror (RoC = -50 mm); GTI—Gires-Tournois-Interferometer mirror; OC—output coupler; GSA—graphene saturable absorber; SESAM—semiconductor saturable absorber mirror, SH—second harmonic output.

In the performed experiments we investigated two different types of saturable absorbers for starting the ML operation. Initially, we employed SESAMs, which acted as an end mirror (cavity length ~ 170 cm). The intracavity beam was focused on the SESAM with a waist radius of $30 \mu\text{m}$. We studied three SESAMs, which varied not only in nonlinear optical parameters, but also in the spectral position of the linear reflectivity band. Throughout the manuscript they will be termed as SESAM 1 (linear reflectivity centered at 1030 nm, modulation depth: 0.4%, recovery time: 500 fs), SESAM 2 (1045 nm, 0.6%, 60 ps) and SESAM 3 (1070 nm, 1%, 10 ps). We also studied the performance of the ML laser using a transmissive GSA. For this experiment, the cavity was extended (~ 175 cm) and the graphene sample was placed at the Brewster's angle in the waist formed by two curved mirrors M_3 and M_4 (see Fig. 1). The size of the beam on the absorber at the waist position amounted to $26 \mu\text{m}$

$\times 32 \mu\text{m}$ and it could have been changed by translating the GSA sample relative to the waist position. The GSA consisted of a chemical vapor deposition-synthesized bi-layer graphene on a 2 mm thick calcium fluoride substrate. Details of the fabrication process as well as characteristics of this sample can be found in [20]. In order to compensate for the normal dispersion of the crystal (560 fs^2 for the double pass [3]) and the CaF_2 substrate (90 fs^2 for the double pass), as well as to balance the effect of self-phase modulation for soliton shaping we employed three Gires-Tournois Interferometer (GTI) mirrors. The amount of the anomalous group delay dispersion (GDD) introduced for the round-trip was experimentally optimized with regard to the pulse duration. For the SESAM ML case it was found to be -1500 fs^2 (6 bounces on -250 fs^2 mirrors). For the GSA ML operation we replaced one of these mirrors with a similar one of -550 fs^2 per bounce, which increased the net value to -2100 fs^2 .

3. Results and discussion

3.1 SESAM mode-locking

We investigated ML operation at first with the 2.6% OC comparing the three SESAMs described in the previous section. The passive mode-locking was always self-starting once the pump power exceeded the threshold value, which in all cases amounted to $\sim 300 \text{ mW}$. The laser emission spectra recorded when using different absorbers are shown in Fig. 2(a). Very similar performance was achieved with SESAMs 1 and 2. For SESAM 1 (2), the laser emitted 24.4 nm (24 nm) broad spectrum centered at 1055 nm (1065 nm). The pulse duration in both cases amounted to 52 fs, which corresponds to a time-bandwidth product of 0.34 (0.33). An exemplary autocorrelation trace (measured for SESAM 1) with a corresponding fit assuming sech^2 -shaped pulses is shown in Fig. 2(b). SESAM 3 produced slightly longer (transform-limited) 59 fs pulses with a spectral bandwidth of 20.5 nm at a central wavelength of 1074 nm. The central wavelength shift can be attributed to differences in linear reflectivity profiles of the SESAMs. However, it is presumably also correlated with the varying absorption bands of the quantum wells for individual absorbers. Yet, this data was not provided by the manufacturer. It is also interesting to note that SESAMs 2 and 3 exhibited long recovery times (60 and 10 ps, respectively). Generation of pulses which are shorter by more than 2 orders of magnitude in these cases confirms that the process responsible for pulse stabilization is soliton mode-locking [21]. Consequently, the pulse parameters were not directly dependent on the absorber, which only helped to initiate the pulsed operation.

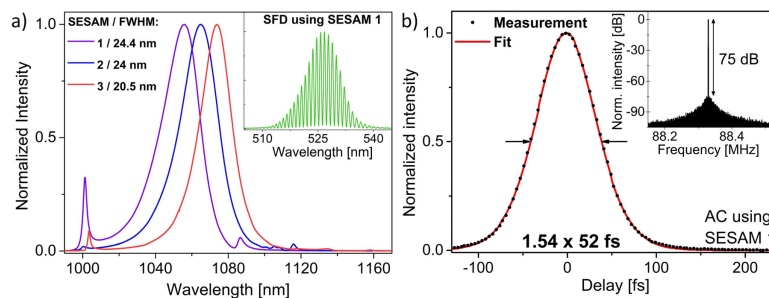


Fig. 2. Performance of the SESAM ML Yb:CNGS oscillator: (a) optical spectra of the pulses for SESAM 1, 2 and 3, FWHM: corresponding emission spectral bandwidths, inset: optical spectrum of the self-frequency doubled (SFD) output generated using SESAM 1; (b) autocorrelation trace (AC) with a fit assuming sech^2 -shaped pulses, inset: the radio frequency spectrum of the fundamental beat note (RBW = 500 Hz) using SESAM 1.

These measurements were performed for the maximum available pump power of 1 W (incident on the crystal) and the output power in all cases amounted to $\sim 75 \text{ mW}$. All laser configurations exhibited similar undisturbed stability—inset of Fig. 2(b) presents an exemplary radio frequency (RF) spectrum (for SESAM 1) of the fundamental beat note at 88.3 MHz

with a signal-to-noise (S/N) ratio of 75 dB. We also characterized the RF spectrum in 3 GHz wide span and did not observe additional parasitic peaks or any other signs of laser instabilities. The additional narrow spectral peaks in Fig. 2(a) occurred due to non-perfect dispersion management. The GDD profile of the employed GTI mirrors was not uniformly flat over the whole emission spectrum. The value of the introduced anomalous GDD was gradually decreasing from 1000 and 1080 nm, to the shorter and longer wavelengths, respectively. This resulted in the appearance of a dispersive wave [21].

We also investigated the performance of the laser with the 0.4% OC, however this did not lead to generation of shorter pulses. The shortest pulse duration (55 fs) was obtained for lower pump power (800 mW). Further increase of the pump power resulted in the appearance of a dominant CW component, rather than broadening of the emitted spectrum.

The tunability of the ML Yb:CNGS laser indicates that the pulse duration is not limited by the emission bandwidth of the crystal, which should readily support sub-50 fs regime. Here, the main limiting factor was not only the low pump power, but also the restrained reflection bands of the employed SESAMs, which prevented from further spectral broadening.

It has been already demonstrated that Yb:CNGS exhibits self-frequency doubling properties [8]. Indeed, we observed second harmonic (SH) generation of the fundamental beam. Due to the low reflectivity of the cavity mirrors in the green, the strongest SH signal could be detected after the folding mirror M_2 . The SH spectrum generated for the oscillator ML with SESAM 1 is shown in the inset of Fig. 2(a). In the employed configuration the SH generation process is non-phase-matched. Under Kleinman symmetry there is a single independent non-zero nonlinear coefficient: d_{11} (defined in an orthogonal frame $\{xyz\}$ where $x \equiv a$ and $z \equiv c$). Although the SFD properties of Yb:CNGS have been already studied [8], its d_{11} coefficient was not determined. Nevertheless, one can assume that it shall be similar to the value measured for the related compound $\text{Ca}_3\text{TaGa}_3\text{Si}_2\text{O}_{14}$ (CTGS), which amounts to 0.72 pm/V [22]. In our experiment, both the azimuthal angle ($\varphi = 0^\circ$) and the angle between the propagation direction inside the crystal and the z -axis ($\theta = 29^\circ$) deviate substantially from the $\varphi = 30^\circ$ value for type-I phase-matching in positive crystals of the point group 32 and the calculated phase-matching angle of $\theta = 36.6^\circ$ [8], respectively. Thus the observed polarization of the SH was the same as that of the fundamental (horizontal, corresponding to type-0, ee-e process) as a result of the sample orientation. The non-phase-matched SH generation in the ML regime results in fringes visible in the spectrum (Fig. 2(a), inset), which is related to the generation of two green pulses in the crystal creating a characteristic interference pattern [23]. The spectral fringe spacing is determined by the group-velocity mismatch between the fundamental and the SH pulses: the experimental value was equal to the calculated one (within the measurement error), which amounts to 1 nm [21]. Naturally, non-phase-matched SH generation is not wavelength-dependent, thus it enabled to convert the entire broadband spectrum of the 52 fs pulses. On the other hand, the efficiency of this process is very low (the coherence length in this configuration amounts to 8.6 μm), thus the average power of the SH beam after the mirror M_2 was $\sim 10 \mu\text{W}$. We have also investigated the non-phase-matched type-I configuration with $\varphi = 30^\circ$ (while maintaining the same θ) by arranging the crystal with its y -axis in the horizontal plane. The SH was polarized along the crystal $x \equiv a$ -axis in this case. Here, the measured conversion efficiency for the ee-o process was approximately 4 times higher than in the previous case due to longer coherence length.

3.2 Graphene mode-locking

Subsequently, we investigated a bi-layer graphene sample as a saturable absorber. Here, the amount of the introduced GDD, which was found to be optimal for the SESAM ML laser, was too low to stabilize the pulsed operation. Consequently, as already mentioned, we increased the total anomalous GDD to -2100 fs^2 per round-trip. After careful alignment of the GSA position, the ML regime was initiated by mechanical perturbation to the M_4 end mirror. The output performance of the laser is shown in Fig. 3. The shortest pulses with a duration of

85 fs were achieved with the 0.4% OC. The corresponding optical spectrum of the transform-limited pulses had a FWHM bandwidth of 14 nm centered at 1064 nm. Additional narrow peaks accompanying the ML spectrum correspond to Kelly sidebands. Their appearance may originate from an additional unsaturated loss periodically introduced by the absorber to the soliton pulse oscillating in the cavity. It also indicates that the net cavity dispersion was close to zero [21]. The difference of introduced GDD between GSA and SESAM mode-locking (600 fs^2 per round-trip) cannot be compensated by the double pass through the CaF_2 substrate (90 fs^2). Consequently, we believe that the SESAMs exhibited an additional intrinsic negative GDD contribution, although such data were not available from supplementary measurements. The RF spectrum of the fundamental beat note at 85.9 MHz with a 72 dB S/N ratio confirms the stability of the pulsed regime. The output power amounted to 23 mW at 600 mW of incident pump power. The mode-locking was self-starting for pump power higher than 700 mW, yet this introduced a pronounced CW peak in the optical spectrum. This parasitic contribution could be then removed by a subsequent decrease of the pump power.

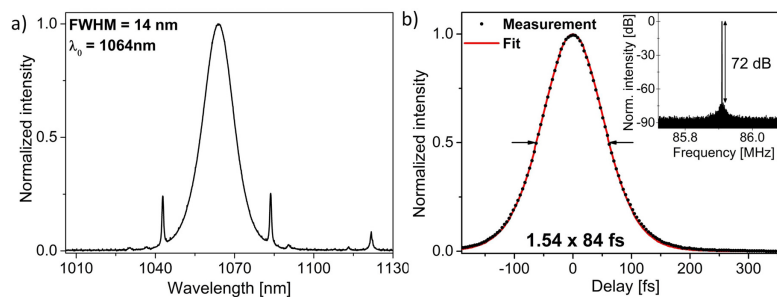


Fig. 3. Performance of the GSA ML Yb:CNGS oscillator: (a) optical spectrum of the pulses; (b) autocorrelation trace with a fit assuming sech^2 -shaped pulses, inset: the radio frequency spectrum of the fundamental beat note (RBW = 500 Hz).

4. Conclusions

We have demonstrated the first ML operation of a laser based on the novel broadband gain medium Yb:CNGS. The single-mode diode-pumped laser was passively ML by a SESAM generating almost transform-limited pulses as short as 52 fs with 75 mW of average output power at ~ 88 MHz repetition rate. By employing SESAMs with different characteristics we obtained stable sub-60 fs operation discretely tunable between 1055 and 1074 nm. The inherent non-phase-matched self-frequency doubling of the fundamental beam in Yb:CNGS has also been characterized. Moreover, we have presented mode-locking with transmissive bilayer graphene as a saturable absorber. In this regime the oscillator emitted 85 fs pulses with output power amounting to 23 mW. Performed investigations confirm that this novel crystal is very attractive for ultrashort pulse generation. The shortest generated 52 fs pulses are still not limited by the intrinsic emission bandwidth of the gain medium, thus we believe that further pulse shortening should be feasible e.g. by employing high brightness pumping. In our future work we will also focus on the SFD properties by investigating phase-matched configurations as well as the possibility to exploit cascaded $\chi^{(2)}$ processes. The calculated spectral acceptance for phase-matched SH generation amounts to ~ 3.2 nm (at the fundamental wavelength) for this particular sample length which will lead to two problems: (i) the SH pulse duration will be lengthened and (ii) the ML laser will try to avoid the frequency conversion losses by operating at a different wavelength. Thus, special efforts will be placed on studying close-to-phase-matching configurations providing sufficient spectral bandwidths with coherent lengths that will ensure practical SH average powers on the mW level.

Funding

National Science Centre (NCN, Poland) (2015/18/E/ST7/00296, 2017/24/T/ST7/00234); Natural Science Foundation of China (51472147, 61178060, 51672161); Natural Science Foundation of Shandong Province (ZR2017MF031); Foundation for Polish Science (FNP, grant no. START 53.2018); Government of the Russian Federation (074-U01) through ITMO Post-Doctoral Fellowship scheme.

References

1. M. Adachi, T. Funakawa, and T. Karaki, "Growth of substituted langasite-type $\text{Ca}_3\text{NbGa}_3\text{Si}_2\text{O}_{14}$ single crystals, and their dielectric, elastic and piezoelectric properties," *Ferroelectrics* **286**(1), 43–48 (2003).
2. I. H. Jung, A. Yoshikawa, T. Fukuda, and K. H. Auh, "Growth and structure of $\text{A}_3\text{NbGa}_3\text{Si}_2\text{O}_{14}$ ($\text{A}=\text{Sr}, \text{Ca}$) compounds," *J. Alloys Compd.* **339**(1-2), 149–155 (2002).
3. X. Zhang, X. Zhang, S. Guo, J. He, K. Han, F. Lou, B. Zhang, R. Wang, and X. Liu, "Growth and optical properties of a new CGG-type laser crystal $\text{Nd}^{3+}:\text{CNGS}$," *Opt. Mater. Express* **5**(5), 977–985 (2015).
4. J. Ren, X. Zhang, X. Zhang, J. Guo, R. Cheng, and S. Guo, "Growth and enhanced electro-elastic properties of $\text{Nd}^{3+}:\text{CNGS}$ crystals with ordered langasite structure," *Mater. Lett.* **167**, 122–124 (2016).
5. J. Ren, X. Zhang, X. Zhang, R. Cheng, J. Guo, X. Zhang, F. Yu, B. Huang, and S. Guo, "Crystal growth, experimental and theoretical studies on the electronic structure of CNGS and $\text{Nd}:\text{CNGS}$," *CrystEngComm* **18**(19), 3481–3487 (2016).
6. X. Zhang, Y. Zhou, A. Yasukevich, P. Loiko, X. Mateos, X. Xu, S. Guo, and Z. Wang, "Diode-pumped passively Q-switched self-frequency-doubled $\text{Nd}:\text{CNGS}$ laser," *Opt. Express* **25**(17), 19760–19766 (2017).
7. J. Li, X.-T. Zhang, J.-L. He, S. Guo, J. Ning, F. Lou, R. Zhao, X.-C. Su, J. Hou, and B.-T. Zhang, "759 fs pulse generation with Nd^{3+} -doped CNGS ordered crystal based on a semiconductor saturable absorber mirror," *Appl. Opt.* **55**(20), 5444–5448 (2016).
8. X. Zhang, Y. Zhou, J. Ren, D. Lu, H. Yu, Z. Wang, S. Guo, and X. Xu, "Growth, thermal and laser properties of a new self-frequency-doubling $\text{Yb}:\text{CNGS}$ crystal," *CrystEngComm* **18**(28), 5338–5343 (2016).
9. X. Zhang, P. Loiko, J. M. Serres, X. Mateos, J. Ren, Z. Wang, S. Guo, X. Xu, E. Vilejshikova, U. Griebner, V. Petrov, M. Aguiló, and F. Díaz, "Highly-efficient laser operation of a novel trigonal silicate crystal $\text{Yb}^{3+}:\text{Ca}_3\text{NbGa}_3\text{Si}_2\text{O}_{14}$," *Opt. Mater. Express* **7**(10), 3626–3633 (2017).
10. X. Zhang, P. Loiko, X. Mateos, J. M. Serres, J. Ren, J. Guo, R. Cheng, C. Gao, Q. Dong, V. Jambunathan, A. Lucianetti, T. Mocek, E. Vilejshikova, U. Griebner, V. Petrov, Z. Wang, S. Guo, X. Xu, M. Aguiló, and F. Díaz, "Crystal growth, low-temperature spectroscopy and multi-watt laser operation of $\text{Yb}:\text{Ca}_3\text{NbGa}_3\text{Si}_2\text{O}_{14}$," *J. Lumin.* **197**, 90–97 (2018).
11. M. J. Lederer, M. Hildebrandt, V. Z. Kolev, B. Luther-Davies, B. Taylor, J. Dawes, P. Dekker, J. Piper, H. H. Tan, and C. Jagadish, "Passive mode locking of a self-frequency-doubling $\text{Yb}:\text{YAl}_3(\text{BO}_3)_4$ laser," *Opt. Lett.* **27**(6), 436–438 (2002).
12. G. I. Stegeman, D. J. Hagan, and L. Torner, " $\chi^{(2)}$ cascading phenomena and their applications to all-optical signal processing, mode-locking, pulse compression and solitons," *Opt. Quantum Electron.* **28**(12), 1691–1740 (1996).
13. M. Zavelani-Rossi, G. Cerullo, and V. Magni, "Mode locking by cascading of second-order nonlinearities," *IEEE J. Quantum Electron.* **34**(1), 61–70 (1998).
14. A. S. Mayer, C. R. Phillips, and U. Keller, "Watt-level 10-gigahertz solid-state laser enabled by self-defocusing nonlinearities in an aperiodically poled crystal," *Nat. Commun.* **8**(1), 1673 (2017).
15. P. Wang, J. M. Dawes, P. Dekker, D. S. Knowles, J. A. Piper, and B. Lu, "Growth and evaluation of ytterbium-doped yttrium aluminum borate as a potential self-doubling laser crystal," *J. Opt. Soc. Am. B* **16**(1), 63–69 (1999).
16. P. Dekker, J. M. Dawes, J. A. Piper, Y. Liu, and J. Wang, "1.1 W CW self-frequency-doubled diode-pumped $\text{Yb}:\text{YAl}_3(\text{BO}_3)_4$ laser," *Opt. Commun.* **195**(5-6), 431–436 (2001).
17. H. Yu, Z. Pan, H. Zhang, and J. Wang, "Recent advances in self-frequency-doubling crystals," *J. Materiomics* **2**(1), 55–65 (2016).
18. Q. Fang, D. Lu, H. Yu, H. Zhang, and J. Wang, "Self-frequency-doubled vibronic yellow $\text{Yb}:\text{YCOB}$ laser at the wavelength of 570 nm," *Opt. Lett.* **41**(5), 1002–1005 (2016).
19. F. Druon, F. Balembois, P. Georges, A. Brun, A. Courjaud, C. Hönninger, F. Salin, A. Aron, F. Mougel, G. Aka, and D. Vivien, "Generation of 90-fs pulses from a mode-locked diode-pumped $\text{Yb}^{3+}:\text{Ca}_4\text{GdO}(\text{BO}_3)_3$ laser," *Opt. Lett.* **25**(6), 423–425 (2000).
20. W. B. Cho, J. W. Kim, H. W. Lee, S. Bae, B. H. Hong, S. Y. Choi, I. H. Baek, K. Kim, D.-I. Yeom, and F. Rotermund, "High-quality, large-area monolayer graphene for efficient bulk laser mode-locking near 1.25 μm ," *Opt. Lett.* **36**(20), 4089–4091 (2011).
21. C. Spielmann, P. F. Curley, T. Brabec, and F. Krausz, "Ultrabroadband femtosecond lasers," *IEEE J. Quantum Electron.* **30**(4), 1100–1114 (1994).
22. F. Chen, F. Yu, S. Hou, Y. Liu, Y. Zhou, X. Shi, H. Wang, Z. Wang, and X. Zhao, "Crystal growth and characterization of CTGS and $\text{Nd}:\text{CTGS}$ for self-frequency-doubling applications," *CrystEngComm* **16**(44), 10286–10291 (2014).

23. P. Trabs, F. Noack, A. S. Aleksandrovsky, A. I. Zaitsev, N. V. Radionov, and V. Petrov, "Spectral fringes in non-phase-matched SHG and refinement of dispersion relations in the VUV," *Opt. Express* **23**(8), 10091–10096 (2015).